Military Technical College
Kobry El-Kobba,
Cairo, Egypt

11-th International Conference
on Aerospace Sciences &
Aviation Technology

COMPUTATIONAL AND EXPERIMENTAL INVESTIGATION OF OPEN CAVITIES FLOW

N. N. Bayomi* and A. M. Abdel Dayem*

ABSTRACT

Computational and experimental investigation was performed for an incompressible flow over an open cavity. A cavity of a unity length-to-depth ratio was considered at Mach number 0.1 and a moderate Reynolds number of 3.18×10^5 based on cavity depth. Different geometries of square and skewed cavities were taken in consideration to investigate their effect on the back flow pressure. The measurements were established for a two dimensional cavity in a wind tunnel of 30 m/s flow velocity corresponding to the considered Mach number. Both the pressure coefficient and the drag coefficient were estimated for the considered geometries. In addition, a numerical simulation of the cavity flow field was developed. A numerical solution of the Navier-Stocks equations was carried out for the incompressible two-dimensional and turbulent flow. The equations were descritized by a finite-element scheme using ANSYS 5.4 code. The flow was fully demonstrated over the cavities considered, acceptable agreement was obtained between the measured and numerical experiments. Moreover, it is found that the square cavity has a less pronounced effect on the back flow than other geometries. The results were verified with the corresponding published data.

KEYWORDS: Experimental cavity flow, open cavity, square and skewed cavities, CFD.

1. INTRODUCTION

The flow within a cavity has received significant attention in view of engineering applications. They include slotted-wall wind and water tunnels, aircraft components, depressions in submarine and ship hulls, computer boards with closely spaced ship carriers, or even the gas dynamic laser

*Faculty of Eng., Mataria, Helwan University, Cairo, Egypt, nnbayomi@hotmail.com
adel_abdeldayem@hotmail.com

cavities. Computational studies concerning cavity flows are usually interested in the flow behavior in shallow cavities with a length-to-depth ratio of 5 or less. In that way, numerical results frequently concern square cavity. Yet, few experiments have been performed to analyze the details of the flow field inside a skewed cavity at low Reynolds number and for low length-to-depth ratio.

Cavity flows, as backward facing step flows, give rise to a complex separated flow generated by a simple geometry. The boundary layer growing upstream from the cavity separates at the cavity lip. A free shear layer begins to develop and reattaches then, either downstream or on the bottom wall of the cavity. Cavity flows are said to be "closed" if the shear layer reattaches on the bottom wall of the cavity and called "open" if not. For a "closed" cavity, it encloses recirculation zones on each side on the cavity. According to Tracy and Plentovich [1], in the supersonic regime, "close" concerns cavities with L/D (cavity length to depth ratio) greater than 13 otherwise it would be an open cavity.

Numerous investigators have carried out the study of the flow field in a rectangular cavity in the past, [Plumbee et al. [2], Pan & Acrivos [3], Metha & Lavan [4], and Heller & Bliss [5]]. Many authors has studied the oscillation mechanisms in shallow cavities and analyzed the deep cavities in supersonic regimes. In fact, several investigators have studied the aeroacoustic phenomenon associated with aerodynamically induced pressure oscillations. These studies are principally aimed to the problem of suppressing the cavity pressure oscillations.

Sarohia [6] observed the development of oscillations in shallow cavities at low subsonic speed. This paper indicated that no acoustic resonance phenomenon appears in the axial direction. The existence of fluctuations in shallow cavities is directly due to the interaction between the shear layer, created upstream at the separation point, and the downstream corner. In addition, Sinha et al. [7] obtained experimentally that the flow in the recirculating region of the shallow open cavity appears to have the character of a wall jet in the reverse direction superimposed on a forward-moving free shear layer.

In the work of Tracy and Plentovich [1], static and fluctuating pressure distributions were obtained along the floor of a rectangular-box cavity. The cavity studied was length-to-height ratios of 4.4, 6.7, 12.67, and 20.0 for yaw angles of 0° and 15° over Mach number range of 0.2 to 0.9 at a Reynolds number of 30×10^6 per foot with a boundary-layer thickness of approximately 0.5 inches. The results indicated that open and transitional-open cavity flow supports tone generation at subsonic and transonic speeds at Mach numbers of 0.6 and above. Cavities that support tone generation at 0° yaw also

supported tone generation at 15° yaw when the flow became transitional-closed.

At low Reynolds number and in a large cavity, the literature seems to be insufficient. Noger et al. [8] performed experiments on a cavity with a length-to-depth ratio of 7.8 and an inlet velocity of 32 m/s ($Re=1.4x10^4$), in order to characterize the flow field and the acoustic phenomena inside the cavity. His results showed the lack of acoustic mode in the cavity and the existence of a shear layer reattachment on the bottom wall.

The flow in rectangular cavities driven by two facing side walls was investigated numerically and experimentally by Kuhlmann et al. [9] for the case when the walls move steadily with equal speed in opposite directions. The flow field organizes into a row of robust rectangular steady cells, which become time-dependent for increasing Reynolds number.

Chung [10] studied the characteristics of transonic rectangular cavity flows. He indicated that the length-to-depth is the most important parameter in determining the characteristics inside the cavity and its vicinity. The length-to-width parameter mainly affects the peak-surface-pressure fluctuation ahead of the rear face. Accordingly, Pereira and Sousa [11] investigated experimentally and numerically unsteady flow oscillations in a shallow rectangular cavity. They considered the incompressible flow for length-to-depth ratio of two. In that manner, Hamed et al. [12] used the direct numerical simulation to investigate transonic flow acoustic resonance in an open cavity.

A neural network-based lumped deterministic source term (LDST) module developed previously representing unsteady effects in quasi-time averaged cavity flow simulations was extended to include cavity length-to-depth (L/D) ratio as a parameter. The characteristics of unsteady cavities were explored as the Mach number varied from 0.3 to 0.7 and the L/D ranged from 1 to 3. These results were computed by Lukovic et al. [13] in times less than two orders of magnitude that required for fully unsteady solutions.

The work of Vakili [14] is a study of a fixed cavity width by depth ratio of 3.33, for four length by depth (L/D) ratios of 2.0, 2.5, 3.5 and 4.5 at subsonic speeds ranging from Mach number equal 0.3 to 0.6. Numerical simulations were performed for cavity geometry configurations and for flows corresponding to the experiments. Experimentally obtained dynamic pressure data show that for cavity with L/D = 2.5, the onset of oscillations occur at a free stream Mach number of about 0.5.

Zdanski et al. [15] studied numerically using the SIMPLER algorithm the influences of the cavity aspect ratios, turbulence level of the oncoming flow, and Reynolds number. They have found that for the turbulent case the

external flow touches the floor of the cavity, and this depends on a specific value of each of these parameters.

Three-dimensional flows in a rectangular channel with a cavity was explained numerically and experimentally by Yamamoto et al. [16]. At high Weissenberg number, the flow in the cavity spirals to move towards the center plane of the channel. In the experiments, the flow of polymer solutions was visualized to observe three-dimensional flow behavior near the cavity part. It was confirmed that the spiraling flow moving towards the center plane emerged in the cavity.

The behavior of structures formed in a cavity strongly depends on the Reynolds number and the cavity length-to depth ratio. In that way, the shear layer pattern seems to respond to these different parameters. The purpose of the present study is to provide insight on the flow behavior in different cavity geometries for inlet velocity condition corresponding to Reynolds number of 3.18×10^5, based on the cavity depth. This cavity is tested for a unity ratio of length-to-depth (L/D=1) and for a width-to-depth ratio W/D=10.5. Different geometries of square and skewed cavities are considered in the present work.

2. EXPERIMENTAL SET-UP AND TEST CONDITIONS

An open circuit boundary layer wind tunnel of the Turbo-machinery laboratory at the faculty of Engineering (Mattaria), Helwan University. It has a working section of 210 x 420 mm by 3250 mm long, as shown in Fig. 1-a. Higazy and Bayomi [17] described more details about the construction of the wind tunnel. The free-stream turbulence level is about 2%, based on the streamwise velocity component, and the streamwise pressure gradient could be controlled by means of a flexible adjustable roof height. The velocity profiles were measured at various streamwise locations on the plate surface, giving an overall view of the entire flow field. The tunnel has a uniform width of 420 mm and an area contraction ratio of 10:1. Downstream of the contraction the height of the working section is 210 mm giving it a 2:1 aspect ratio at inlet. The cavities were fixed at 1460 mm from tunnel inlet.

The static pressures in the cavity were measured referenced to the tunnel static pressure with a high precision calibrated digital micromanometer model Yokogawa 2655, having a measured range of –1000 mm of H_2O with an accuracy of $\pm$0.4%. As the pressure readings fluctuate with time, readings are recorded by a personal computer using an A/D converter and an average of readings is computed every 5 sec. The resulting reading signals were fed into a computer program, which integrate the raw data. The flow chart of data processes is shown in Fig. 1-b. Different configurations for tested cavities are shown in Fig. 2. The depth of cavity, D is 40 mm and the base length is 40

mm. The width of the cavity is kept constant and equal 420 mm. The length-to-depth ratio is 1.0 and the width-to-depth ratio is 10.5.

The different cavity geometries are shown in Fig. 2 with their corresponding dimensions. The first cavity is square shape with length and depth of 40 mm and width that equals the tunnel width. The second and third cavities are skewed cavities, the cavity two sides are sloped 45° on the channel flow direction. The side walls are sloped to the right in cavity (2) where they sloped to left in cavity (3). In cavity (4) the right side wall is only sloped 45°to the channel flow direction while the left side wall is sloped 45°to the flow direction in cavity (5). The full dimensions of each cavity considered are presented in Fig. 2.

The cavities with different geometries were manufactured all of wood with polished inside surfaces to minimize the flow friction. Each cavity was carefully tightened by its opening through an opening of a flat wooden sheet that is fixed inside the roof of the wind tunnel. The wooden sheet has the same flat level of the tunnel roof and it is carefully tightened with it to let any air ventilation around both sheet and cavity. After the measurements the cavity was replaced with others simultaneously. Plate 1 indicates clearly the experimental samples of the cavities considered.

The static taps 1 mm diameter were fixed on the center line through the cavity width. The taps were tightened inside holes on the cavity walls and roof, the distance between any two holes is 10 mm. The taps were connected to rubber tubes to measure the pressure by the digital micromanometer.

3. COMPUTATIONAL MODELING

A two-dimensional numerical modeling of the flow inside and over the cavities was performed by the ANSYS 5.4 code that is based on the finite element technique. Steady-incompressible and turbulent flow was considered for all cases of flow cavities. The governing differential equations of Navier-Stokes for Newtonian fluid and numerical solution as indicated in the code are as follows:

3.1 Continuity Equation

From the law of conservation of mass law, it comes the continuity equation:

$$\frac{\partial \rho}{\partial t} + \rho \frac{\partial (V_x)}{\partial x} + \rho \frac{\partial (V_y)}{\partial y} = 0 \qquad (1)$$

Where: V_x, and V_y = Components of the velocity vector in the x, y directions, respectively

x and y = Global Cartesian coordinates
t = Time
ρ = Density

The rate of change of density can be replaced by the rate of change of pressure and the rate at which density changes with pressure:

$$\frac{\partial \rho}{\partial t} = \frac{\partial \rho}{\partial p}\frac{\partial p}{\partial t} \tag{2}$$

Where p is the flow pressure. The evaluation of the derivative of the density comes from the equation of state. The pressure waves are assumed to be traveled infinitely fast throughout the domain ($d\rho/dp=10^{-5}$)

The momentum equations, without further assumptions regarding the properties, are as follows:

$$\frac{\rho\,\partial V_x}{\partial t} + \frac{\rho\,\partial(V_x V_x)}{\partial x} + \frac{\rho\,\partial(V_y V_x)}{\partial y} = \rho g_x - \frac{\partial P}{\partial x} + R_x + \frac{\partial}{\partial x}(\mu_e \frac{\partial V_x}{\partial x}) + \frac{\partial}{\partial y}(\mu_e \frac{\partial V_x}{\partial y}) + T_x \tag{3}$$

$$\frac{\rho\,\partial V_y}{\partial t} + \frac{\rho\,\partial(V_x V_y)}{\partial x} + \frac{\rho\,\partial(V_y V_y)}{\partial y} = \rho g_y - \frac{\partial P}{\partial y} + R_y + \frac{\partial}{\partial x}(\mu_e \frac{\partial V_y}{\partial x}) + \frac{\partial}{\partial y}(\mu_e \frac{\partial V_y}{\partial y}) + T_y \tag{4}$$

Where g_x & g_y = Components of acceleration due to gravity.
R_x & R_y = Distributed resistance.
T_x & T_y, = Viscous loss terms.
μ_e = Effective viscosity.
ρ = Flow density.

$$T_x = \frac{\partial}{\partial x}(\mu \frac{\partial V_x}{\partial x}) + \frac{\partial}{\partial y}(\mu \frac{\partial V_y}{\partial x}) \tag{5}$$

$$T_y = \frac{\partial}{\partial x}(\mu \frac{\partial V_x}{\partial y}) + \frac{\partial}{\partial y}(\mu \frac{\partial V_y}{\partial y}) \tag{6}$$

Then the partial differential equations solved in the Launder and Spalding [18] two-equation model are as follows:

$$\frac{\rho\,\partial k}{\partial t} + \frac{\rho\,\partial(V_x k)}{\partial x} + \frac{\rho\,\partial(V_y k)}{\partial y} = \frac{\partial}{\partial x}(\frac{\mu_t}{\sigma_k}\frac{\partial k}{\partial x}) + \frac{\partial}{\partial y}(\frac{\mu_t}{\sigma_k}\frac{\partial k}{\partial y}) + \mu_t \Phi - \rho\varepsilon + \frac{C_4\,\beta\,\mu_t}{\sigma_t}(g_x \frac{\partial T}{\partial x} + g_y \frac{\partial T}{\partial y}) \tag{7}$$

$$\frac{\rho \partial \varepsilon}{\partial t} + \frac{\rho \partial (V_x \varepsilon)}{\partial x} + \frac{\rho \partial (V_y \varepsilon)}{\partial y} = \frac{\partial}{\partial x}\left(\frac{\mu_t}{\sigma\varepsilon} \frac{\partial \varepsilon}{\partial x}\right) + \frac{\partial}{\partial y}\left(\frac{\mu_t}{\sigma_\varepsilon} \frac{\partial \varepsilon}{\partial y}\right) + C_1 \mu_t \frac{\varepsilon}{k} \Phi - C_2 \rho \frac{\varepsilon^2}{k} + \frac{C_1 C_\mu C_3 \beta \rho k}{\sigma_t}\left(g_x \frac{\partial T}{\partial x} + g_y \frac{\partial T}{\partial y}\right) \quad (8)$$

Where k = Turbulent kinetic energy.
ε = Turbulent kinetic energy dissipation rate.
Φ = Flow variable.
β = Input quantity.

The two equation turbulence model of Launder and Spalding [18] is used to evaluate the turbulent viscosity (μ_t) through the expression:

$$\mu_t = C_\mu \rho \frac{k^2}{\varepsilon} \quad (9)$$

The final term in each equation is used to model the effect of buoyancy. Launder and Spalding [18] provided default values for the various constants in the model, see Table 2.

Table 2. Values for various constants in the model

Value	C_1	C_2	$C\mu$	σ_k	$\sigma\varepsilon$	σ_t	C_3	C_4
Default	1.44	1.92	0.09	1	1.3	1	0	0

3.2 Boundary Conditions

The inlet velocity has a component in the x direction of 30 m/s, the velocity component in the y direction equals to zero. Also, all velocity components were taken zero value on the upper and lower domain boundaries and on the cavity walls as well. The outlet conditions of the domain were limited to 785 Pa pressure that was measured across the working section of the tunnel. These boundary conditions are enough to solve the governing equations to estimate the flow primitive variables, pressure and velocity for each element inside the computational domain.

3.3 Numerical Solution

A two-dimensional numerical modeling of the flow over the considered cavities was performed by the ANSYS 5.4 code that is based on the finite element technique. The computational domain is a rectangle located over the cavity with area of 440 mm long and 200 mm width. The center of the cavity opening is located at x = 220 mm and y = 40 mm in the domain from the left

corner. The computational domain of each cavity is presented in Figs. 3 a, b & c.

First of all a grid generation of the domain was established with grid refinement inside the cavity and in the area located over the cavity. The triangular grids were used with fine mesh inside the cavity and in the area above. That can accelerate the solution convergence and avoid numerical errors in that area. Accordingly, the grid distribution can be controlled inside the domain. The number of grids was 4977, 5811, 5811, 6398 and 6398 elements for the cavities number. 1, 2, 3, 4 and 5 respectively. However, the size of the elements is changed according to the concentration of the grids. Figures 3 a, b & c explain the grid concentration inside the domain for the considered cases.

The steady solution of the Navier-Stokes equations was developed in iterative sequence starting with initial values of the variables to reach the convergence solution. A number of solution iterations can be determined, 100 iterations were taken in consideration for all solved cases. This number of iterations obtained a converged and stable solution for all cases. The convergence solution spent few minutes by Pc computer for all problems that reached up to 10 minutes. The computational time can be considered very small for such computational aerodynamic applications.

To accommodate the varying accuracy requirements, two types of solvers are provided, both types are iterative. The first is a sweeping method that is known as the Tri-Diagonal Matrix Algorithm (TDMA) and the second is semi-direct solver known as conjugate direction method. TDMA is used to obtain the approximate solution and the conjugate direction method is used when exact solution is needed.

The method of breaking the problem into a series of tri-diagonal problems where any entries outside the tri-diagonal portion are treated as source terms using the previous values. For a completely unstructured mesh, or an arbitrary numbered system, the method reduces to the Gauss-Seidel iterative method.

The conjugate gradient method is pre-conditioned with an incomplete decomposition and is used only for the pressure equation of incompressible flows. The sequential solution algorithm must allow space for a non-symmetric coefficient matrix for the momentum and energy equations. Only half this storage is required for the symmetric matrix and the other half is used to store the decomposition. The conjugate residual method can be used with or without preconditioning, the latter approach requiring significantly less computer memory. The user specifies a convergence criterion and maximum number of iterations.

4. NUMERICAL RESULTS AND DISCUSSION

The computational domain for the airflow through the channel with a cavity to approaching flow was schematically shown in Figs. 3-a, b & c with grid configurations. The discretization method used in the present study uses a finite element formulation. The primitive variables of the flow; pressure and velocity were estimated for each node in the domain and the results are given in the form of contour plots and vector plots respectively as shown in the Figs. 4 to 8. The code allows also finding the distribution of the flow variables in any predefined path inside the domain. By this advantage, the pressure was determined on the cavity walls as presented in Fig. 9, compared with the corresponding experimental ones.

The velocity vectors and pressure contours are presented for the different cavities flow in the figures from 4 to 8. For the square cavity shown in Figs. 4 a & 4d, the flow is considered as an open cavity flow. The flow essentially bridges the cavity, a shear layer is formed over the cavity. A recirculation region is observed inside the cavity. The pressure increases near the cavity floor and it is increased gradually into the downstream edge. This conclusion is verified clearly by the work of Yamamoto et al. [16] and Zdanski et al. [15]. The flow visualization in these studies are completely in agreement with present work as can be indicated from Figs. 4 a, 4b & 4c.

A nearly uniform static pressure distribution is produced, however high intensity acoustic tones can develop. These tones can induce vibrations in the surrounding structure, including the separating store and lead to structural fatigue. This result can be relatively accepted according with the results of Tracy and Plentovich [1] for the case of open cavity. The mechanism that produces acoustic tones for open cavity flow fields is understood as indicated by Tracy and Plentovich [1] to be a re-enforcement between instabilities in the shear layer that bridges the cavity and pressure waves. They are generated in the cavity when the shear layer impinges on the aft wall. Acoustic tones occur at discrete frequencies that correspond to characteristic pressure patterns (standing waves or modes) in the cavity.

A conclusion should be noted that, the flow in the considered open cavities at subsonic region is similar to the flow at supersonic region indicated in Tracy and Plentovich [1]. This indicates that, the cavity under supersonic flow can be considered as an open cavity. A similar flow of the square cavity is found for the skewed cavity 2 that is indicated in Figs. 5a & 5b. The flow vorticity is presented inside the cavity and the flow bridges the cavity. The pressure is slightly increased inside the channel, the maximum pressure equals 894 Pa where it is 744 Pa for the cavity 1. In general there is no big difference in the results of both cavities, the pressure is slightly changed in the bottom of the

domain. In Figs. 6a & 6b of the cavity 3, while the flow is inversed from right to left (opposite of cavity 2) it is slightly changed, the maximum pressure reaches about 780 Pa around the cavity trailing edge while the velocity vectors are relatively not changed. The cavity leading edge is interchanged by trailing edge of the cavity 2.

Figures 7a & 7b show the flow of the skewed cavity 4. In this cavity, the leading side is vertical and the trailing side is inclined 45° on the flow direction. The trailing side wall is such as in the cavities 2 and 3. Therefore, the flow over the cavity is similar to the last two cavities. The recirculation region is moved into a part of the cavity that changed from cavity 1 and cavity 2 (or 3). There is no significant effect on the channel flow. Accordingly, the cavity 5 has the same geometry of cavity 4; the flow direction is only changed from left to right. This also exchanges the leading side into trailing side and vice versa as in the cavities 2 and 3, so the flow is changed gradually as before. The maximum flow is increased from 882 Pa for the cavity 4 into 934 Pa for the cavity 5, as shown in Figs. 8 a & 8 b.

From the above presentation, it can be noted that the leading edge shape of the cavity has a significant effect on the cavity flow. It causes the flow circulation or eddies that appear inside the cavity. The cavity flows driven by separated boundary layer are reattached or relaxed flow. In the square cavity, the boundary layer is controlled by a transverse mechanism, while in the skewed cavity, the separated boundary layer is controlled by a longitudinal mechanism. There are different vortex structures associated with the transverse and longitudinal mechanism. The flow in a skewed cavity in a longitudinal fashion is characterized by a large trailing edge vortex. The cavity flow appears as a jet in the reverse direction superimopsed on a forward-moving free shear layer as indicated by Sinha et al. [7].

With the onset of the longitudinal mechanism, the magnitude of the transfer rises sharply. The longitudinal cavity flow has a large influence downstream, the orderly vortical structures, which are generated by the vortices and the boundary layer spanning the cavity. In a skewed cavity, the pressure is characterized by the large vortex stationed near the trailing edge. In the mean time, the large downward boundary layer deflection causes a recompression near the trailing edge of the cavity and subsequently a pressure rise in the downstream half of the cavity. The onset of the longitudinal mechanism is expected to increase the form drag of the cavity.

Cavities such as weapons bays or automobile door gaps can sustain unsteady oscillations without external excitation. At subsonic speeds, cavities can be classified as responding in either "shear-layer mode" or "wake mode". In shear-layer mode, the shear layer spans the mouth of the cavity and stagnates at the aft wall. This is clearly presented in Figs 4d, 5b, 6b, 7b & 8b.

In wake mode, the cavity is characterized by large-scale vortex shedding and flow stagnation on its floor. However, in the wake mode, self-excited oscillations cease, the cavity flow becomes unstable and the drag due to the presence of the cavity greatly increases. In the literature, vastly different values have been reported for the cutoff ratio, but generally, short and deep cavities were considered to be in "shear-layer mode". This conclusion agrees with our results. Moreover, Tracy and Plentovich [1] concluded that the disagreement found in the literature stems from the dependence on both length-to depth ratio and Mach number.

5. EXPERIMENTAL VALIDATION OF THE NUMERICAL RESULTS

The five considered cavities are investigated also in the experiments. The pressure was measured on the cavity sides and floor, it was measured on the mid-span of the cavity. Typical measured and numerical surface pressure distributions for five cavities are presented in Fig. 9. The cavities tested here are of the open types as described before. The major mechanisms dominate the surface pressure inside the cavity, namely vortices in the cavity, the boundary layer impingement, and the recompression of the flow near the trailing edge of the cavity. When the cavity is deep, the recompression of the flow and the momentum diffusion across the boundary layer become increasingly important. These results in a pressure rise on the floor of the cavity which occurs well before the downstream corner of the cavity.

Regarding the comparison between the numerical and experimental data, the pressure distribution on the cavity walls was estimated as shown in Fig. 9. The pressure was estimated on the leading and trailing sides and the cavity floor as well. Because two-dimensional analysis was considered in this study, the cavity walls are considered as lines named AB for leading side (upstream face), BC for the floor and CD for the trailing side (downstream face). The figure presents both the pressure calculated and measured on these lines. The experimental values were measured on the span lines of the cavity walls.

The pressure distribution was demonstrated in the form of a pressure coefficient as defined in the nomenclature. In general the difference between the measured and numerical results can be accepted, it ranges up to 15% in average. The difference is obtained from the sensitivity of the measured data which is affected by the flow separation and fluctuation. This can be seen near the cavity corners and in the critical areas. That can be noted for all cavities and sidewalls. In addition, using of Launder and Spalding turbulence-model may obtain certain of accuracy near the walls. Also, the boundary conditions were considered constant values at each side in the numerical modeling and this is not actually true. The pressure coefficient was estimated on the cavity floor by Zdanski et al. [15] for Re = 662. The difference between the present

work and published data is due to difference in conditions of the flow. The Reynolds numbers are different in two cases. The pressure distribution is relatively straight line of all cavity sides for all cavities considered. The cavity walls are equally affected by the flow. In addition, the pressure difference between the cavities is not significant for the cavity sides.

The drag coefficients of the cavity estimated from the pressure difference along the upstream (front) and downstream (back) faces of the cavity are presented in Fig. 10. Simultaneously, the pressure on the downstream face of the cavity rises due the recompression of the flow and a large downstream deflection of the boundary layer near the trailing edge of the cavity. This brings the dividing streamline down towards the floor of the cavity and subsequently causes an increased dynamic pressure towards the stagnation point. The combined effects are to increase the drag coefficient. When the cavity is skewed, the momentum diffusion begins to play an important role in determining the mass and momentum balances of the cavity flow. The onset of the boundary layer is expected to bring additional momentum into the cavity, which would increase the drag of the cavity as shown for skewed cavities in Fig. 10. Finally, the numerical values of C_D are well validated by the experimental ones. The square cavity has the lowest drag coefficient (C_D) of all cavities with less drag force. Changing the cavity side to be skewed increases (C_D) as in cavity 2 and 3.

7. CONCLUSION

Experimental and numerical investigation of the flow over different geometries of square and skewed cavities were presented. The pressure and drag coefficients were estimated experimentally. They are in good agreement with the numerical data. The flow was clearly investigated on the cavity walls and in the region above it.

The following remarks have been concluded:

1-The square and skewed cavities flow driven by strong adverse pressure gradient are two types; transverse for square cavities and longitudinal for skewed cavities.

2- Detailed numerical presentation of the cavity flow was obtained and it is in good agreement with experimental demonstration and published data.

3- The square cavity has a lower drag coefficient than the skewed geometries.

REFERENCES

[1] Tracy, M. B. and Plentovich, E. B., Characterization of cavity flow fields using pressure data obtained in the langley 0.3-meter transonic cryogenic tunnel" NASA Technical Memorandum, pp 4436, (1993).
[2] Plumbee H. E, Gibson J. S. and Lassiter L.W., A theoretical and experimental investigation of the acoustic response of cavities in an aerodynamic flow, WADD-TR, pp 61-75, (1962).
[3] Pan. F. and Acrivos A., Steady flows in rectangular cavities, Journal of Fluids Mechanics, Vol.28, Part.4, pp. 643-655, (1967).
[4] Metha, U. B. and Lavan, Z., Flow in a two-dimensional channel with a rectangular cavity , NASA CR 1245, (1969).
[5] Heller, H. H. and Bliss D.B., Aerodynamically induced pressure oscillations in cavities- Physical mechanisms and suppression concepts, AFFDL-TR-74-133, 1975.
[6] Sarohia, V., Experimental investigations of oscillations in flows over shallow cavities, AIAA J., Vol.15, No.5, pp.984-991, (1977).
[7] Sinha, S. N., Gupta, A. K. and Oberai, M. M., Laminar separating flow over backsteps and cavities, Part II: Cavities, AIAA J., Vol. 20, No. 3, pp. 370-375, (1982).
[8] Noger, C., Lazure, H. and Patrat, J. C., Etude aéroacoustique d'une cavité peu profonde soumise à unécoulement affleurant , 14ème Congrès Français de Mécanique, Toulouse, France, (1999).
[9] Kuhlmann, H. C. Albensoeder, H. and Blohm, C., Flow instabilities in the two-sided lid-driven cavity, 12th International Couette-Taylor Workshop, September 6-8, Evanston, IL USA, (2001).
[10] Chung K., Characteristics of transonic rectangular cavity flows, Journal of Aircraft, Vol. 37, No. 3, pp. 464-467, (2000).
[11] Pereira, J. C. F. and Sousa, J. M. M., "Experimental and numerical investigation of flow oscillations in a rectangular cavity, Transactions of the ASME, Vol. 117, pp. 68-74, (1995).
[12] Hamed, A., Basu, D. and Das, K., Numerical simulations of transonic flow acoustic resonance in cavity, Proceedings of Seventh International Congress on Fluid Dynamics and Propulsion, December 18-20, Cairo, Egypt, ICFDP7-2001059, (2001).
[13] Lukovic, B. Orkwis, P. D. and Turner, M. G., Effect of cavity l/d variations on neural network-based deterministic unsteadiness source terms, AIAA 2002-0857, (2002).
[14] Vakili, A. D., An experimental and numerical study of open cavity flows, Thesis Ph. D., University of Tennessee, Knoxville, (2002).
[15] Zdanski, P. S. B., Ortega, M. A., Nide, G. C. R. & Fico Jr., Numerical study of the flow over shallow cavities, J. Computers & Fluids 32, pp. 953–974, (2003).

[16] Yamamoto, T., Ishiyama, M., Nakajima, M., Nakamura, K., & Mori, N., Three-dimensional viscoelastic flows through a rectangular channel with a cavity, J. Non-Newtonian Fluid Mech. 114, pp. 13–31, (2003).
[17] Higazy, M. G. and Bayomi, N. N., Experimental investigation of flow field characteristics over two cavities in tandem, 11th International Mechanical Power Engineering Conf. (IMPEC 11), Helwan University, Faculty of Engng., Mataria, 5-7 Feb., Cairo, Egypt, (2000).
[18] Launder, B. E. and Spalding, D. B., The numerical computation of turbulent flows, Computer Methods in Applied Mechanics and Engineering, Vol. 3, pp. 269-289, (1974).

Nomenclature

C_D Drag coefficient, $C_D = \int_{y=0}^{y=D} \{p_f(y) - p_b(y)\} dy / (0.5 \rho U^2 D)$

Cp Pressure coefficient, $C_p = \frac{p_{(st)} - p_{(y)}}{q_\infty}$

D	Groove depth
L	Cavity length
l	Groove length in the streamwise direction
p	Flow pressure
$p_{(y)}$	Surface static pressure
p_{st}	Static pressure on groove walls and floor
q_∞	Free-stream dynamic pressure
Re	Reynolds number
T_x & T_y,	Viscous loss terms.
t	Time
U	Mean flow velocity
V	Directional flow velocity
x	Axial distance measured from the wall
y	Normal distance measured from the wall
w	Cavity width
z	Distance normal to x-y plan
ρ	Fluid density

Subscript

b Back face
f Front face
i Inclined face
x X-direction
y Y-direction

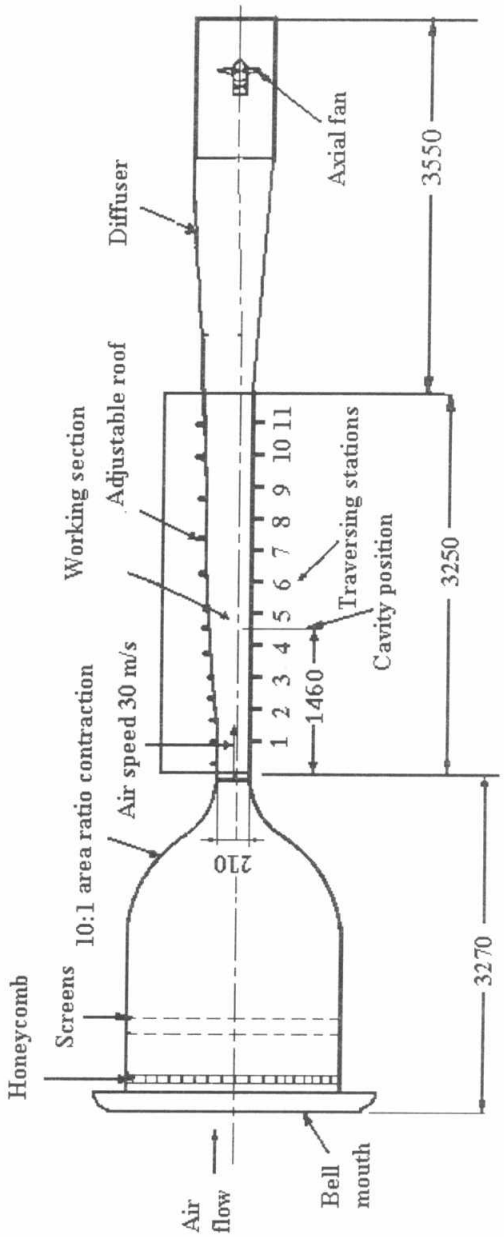

Fig. 1 a Boundary layer wind tunnel, dimensions in mm.

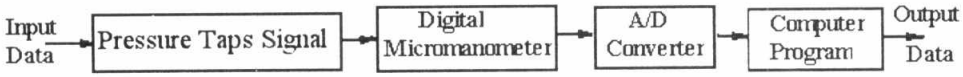

Fig. 1 b. Flow chart of the data evaluation process.

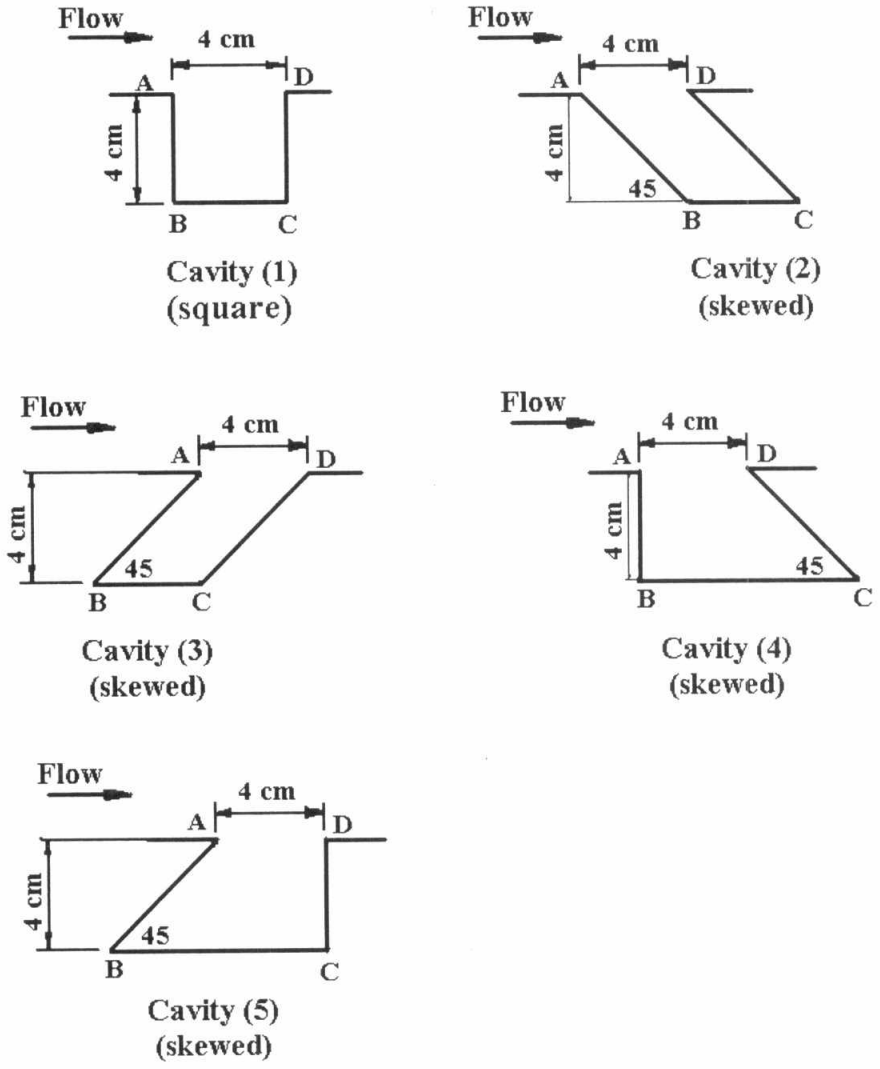

Fig. 2. Geometry of cavities used in the present investigation.

Cavity 2 Cavity 4 Cavity 1

Plate 1. Photograph of samples of cavities considered.

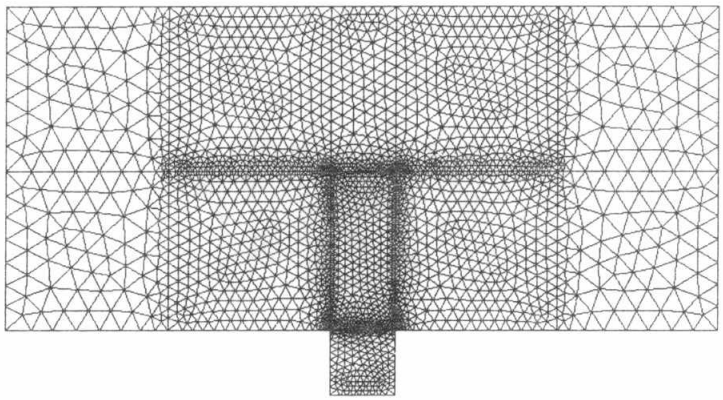

Fig. 3a. Mesh generation of cavity 1 with 4977 triangular grids.

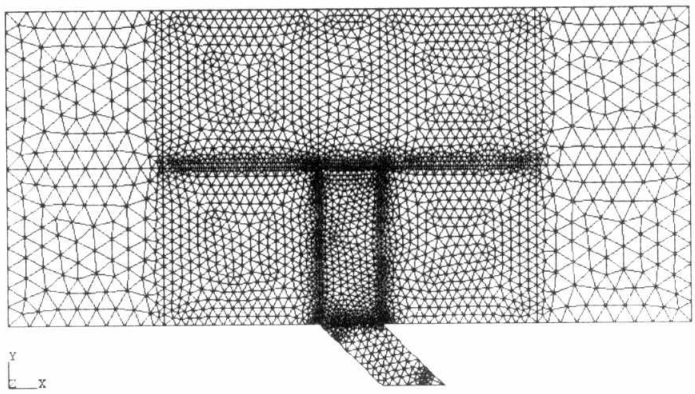

Fig. 3b. Mesh generation of cavities 2 &3 with 5811 triangular grids.

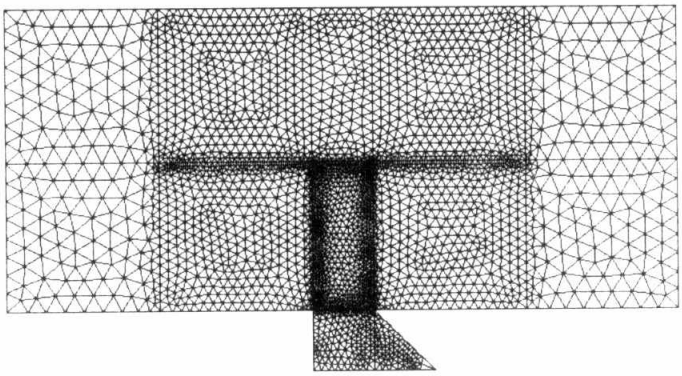

Fig. 3c. Mesh generation of cavities 4 & 5 with 6398 triangular grids.

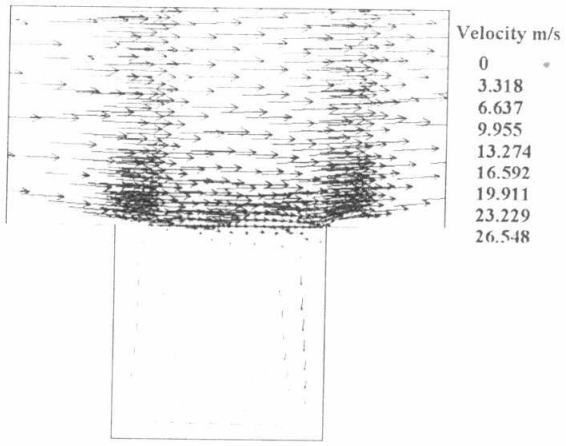

Fig. 4a. Velocity vectors of the cavity 1 ($Re=3.18x10^5$).

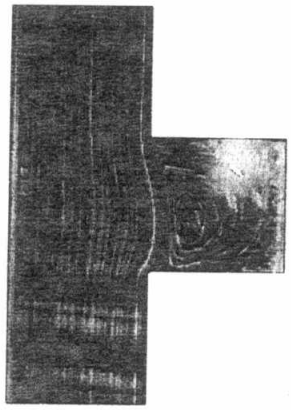

Fig. 4b. Experimental visualization of a cavity flow, l/D=6, square cavity, Yamamoto et al. [16].

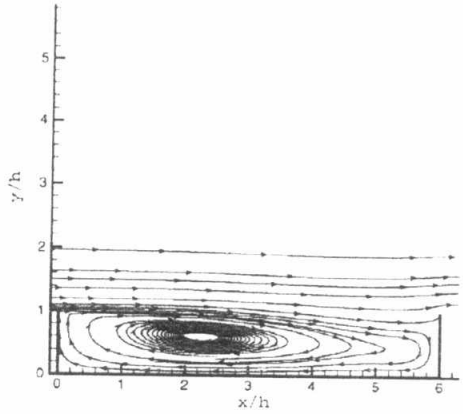

Fig. 4c. Streamlines of the Re=662, Zdanski et al. [15].

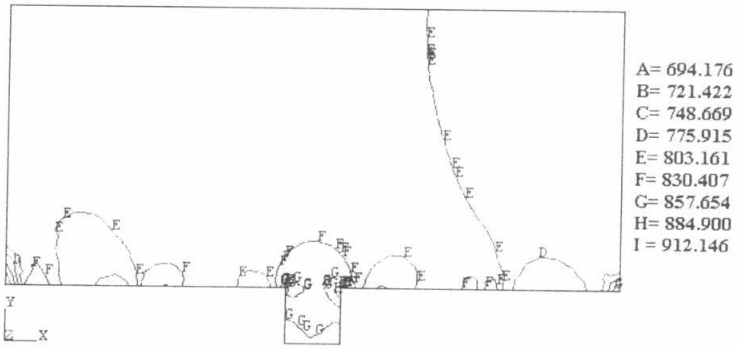

Fig. 4d. Pressure contours of the cavity 1 ($Re=3.18x10^5$).

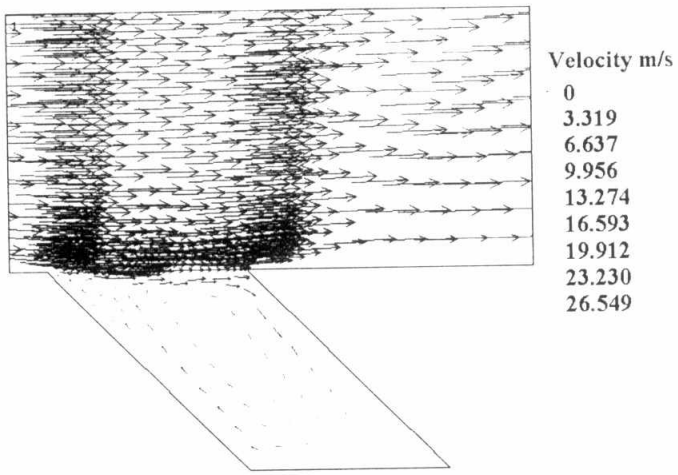

Fig. 5a. Velocity vectors of the cavity 2 ($Re=3.18x10^5$).

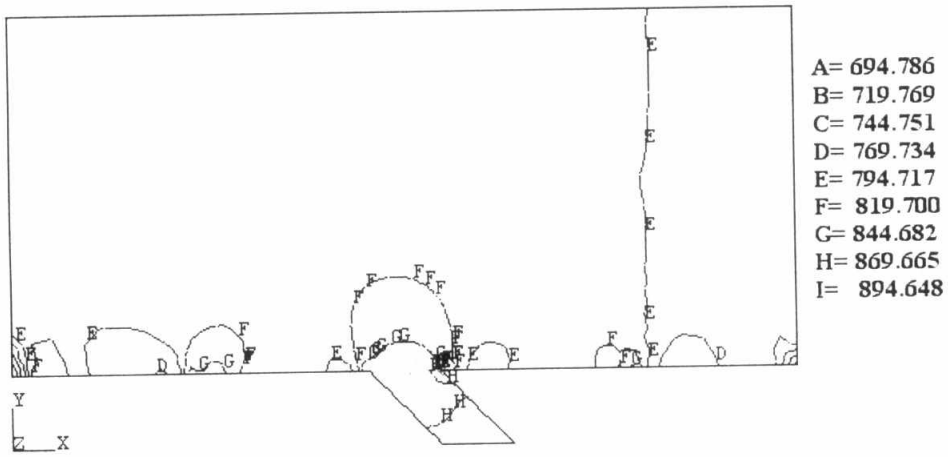

Fig. 5b. Pressure contours of the cavity 2 ($Re=3.18x10^5$).

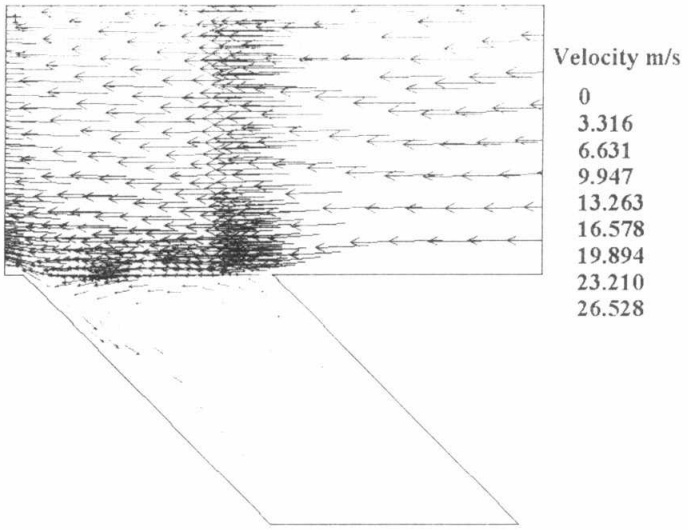

Fig. 6a. Velocity vectors of the cavity 3 ($Re=3.18x10^5$).

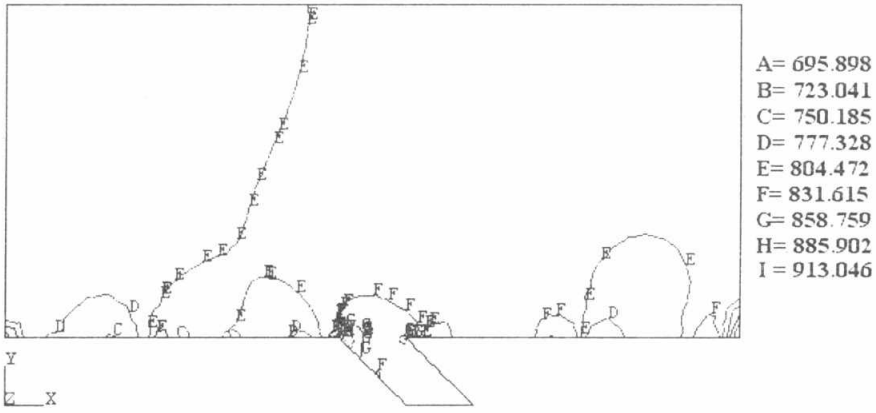

Fig. 6b. Pressure contours of the cavity 3 ($Re=3.18x10^5$).

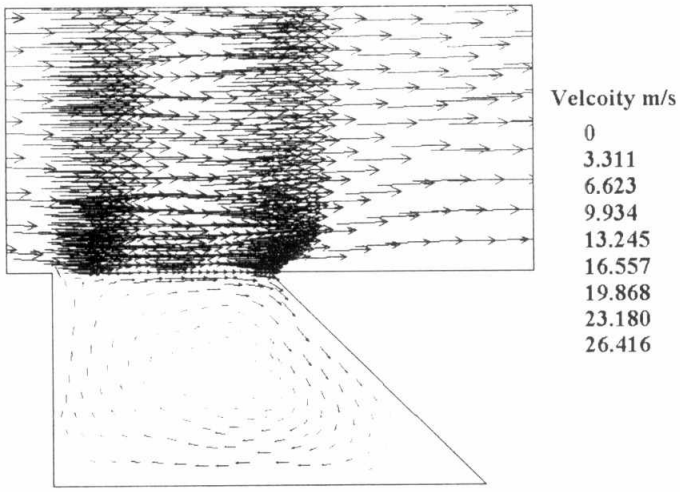

Fig. 7a. Velocity vectors of the cavity 4 ($Re=3.18x10^5$).

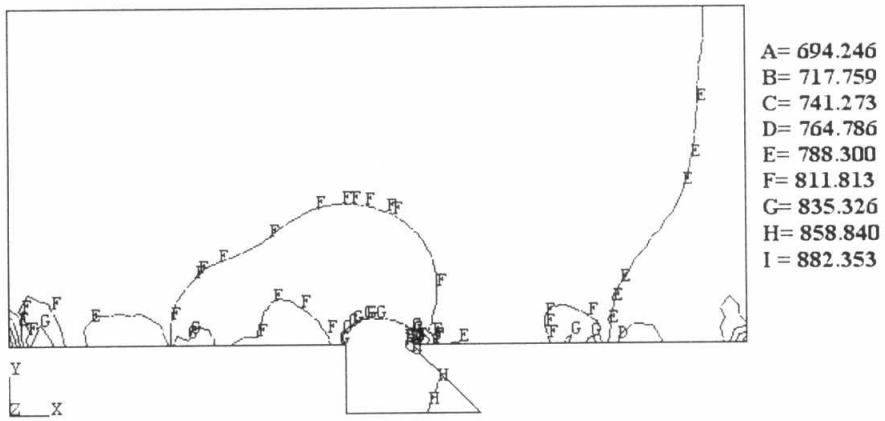

Fig. 7b. Pressure contours of the cavity 4 ($Re=3.18x10^5$).

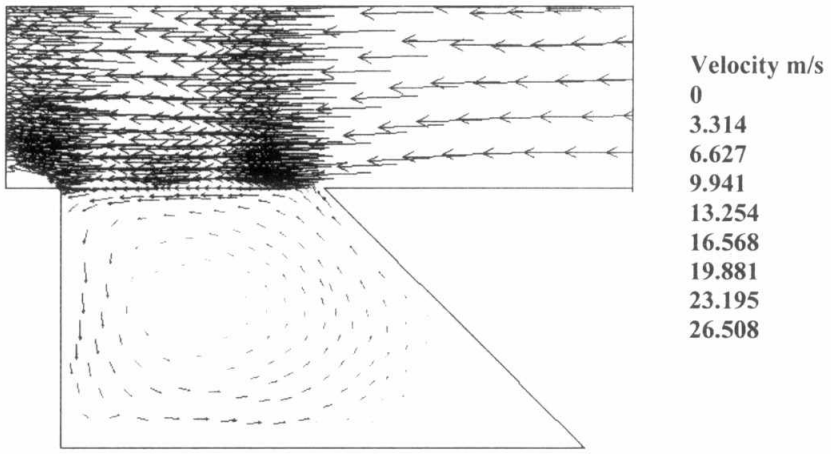

Fig. 8a. Velocity vectors of the cavity 5 ($Re=3.18x10^5$).

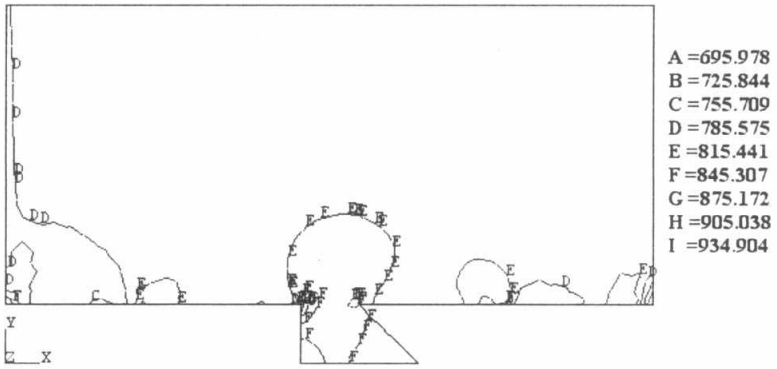

Fig. 8b. Pressure contours of the cavity 5 ($Re=3.18x10^5$).

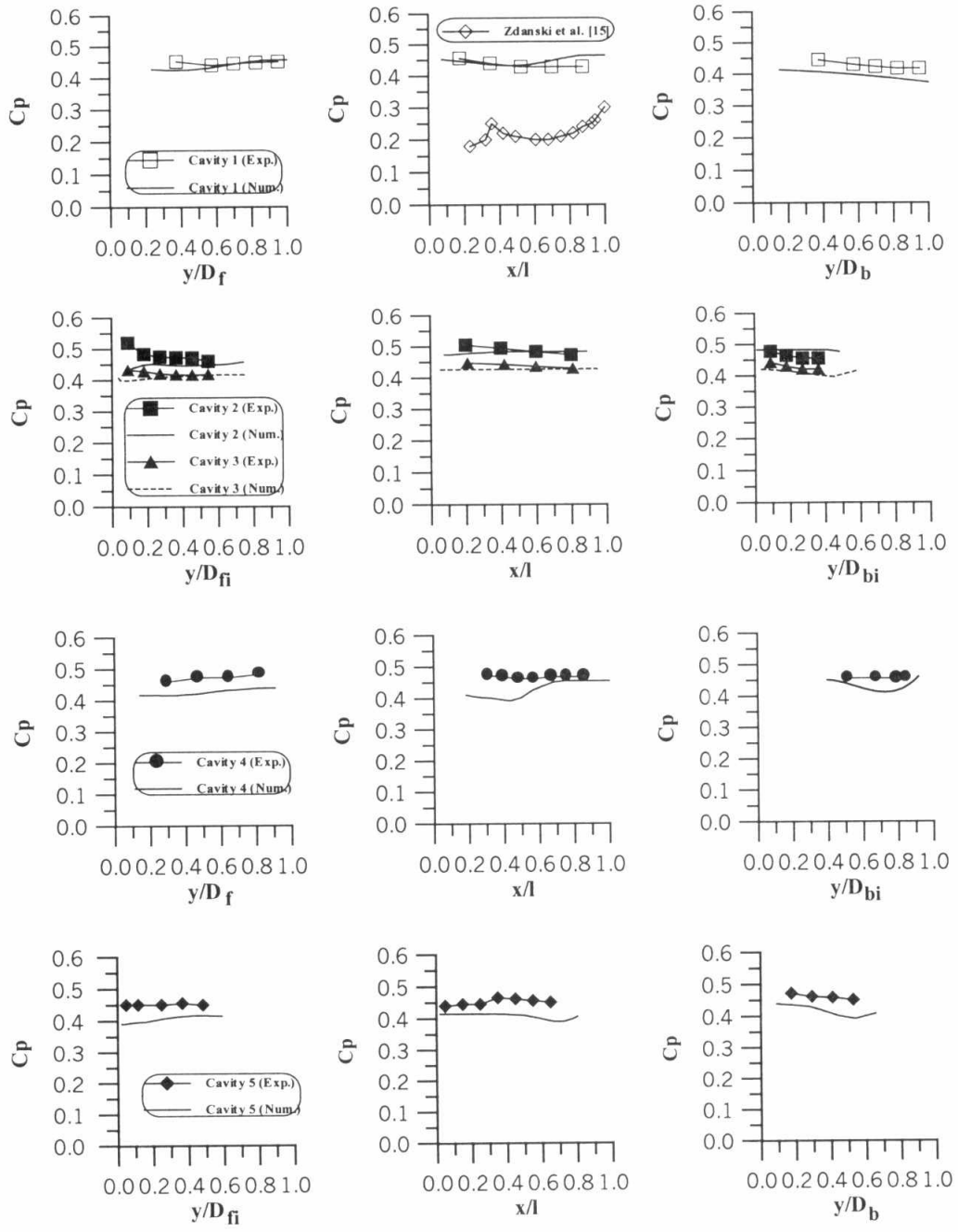

Fig. 9. Numerical and experimental surface pressure coefficient (Re=3.18x10^5).

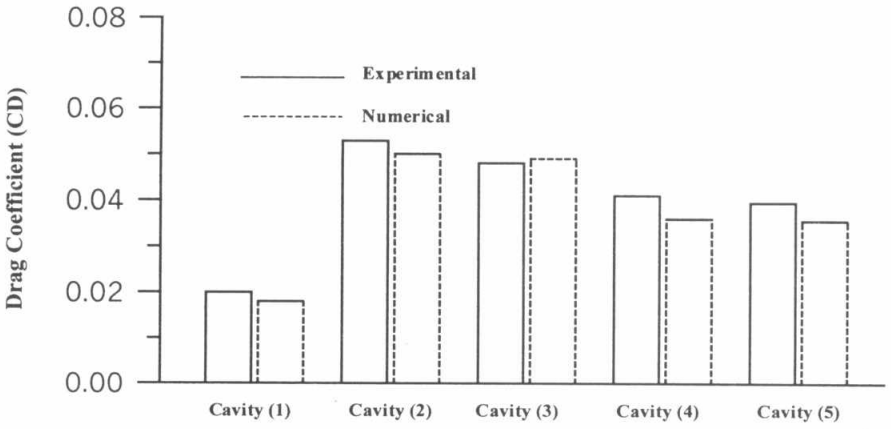

Fig. 10. Effect of the cavity geometry on the drag coefficient ($Re=3.18x10^5$).